Role of the Berry Phase in the Formation of Stripes in Manganese Oxides*

Takashi Hotta† and Yasutami Takada
Institute for Solid State Physics, University of Tokyo, 7-22-1 Roppongi, Minato-ku, Tokyo 106-8666, Japan

Hiroyasu Koizumi
Faculty of Science, Himeji Institute of Technology, Kanaji, Kamigori, Ako-gun, Hyogo 678-1297, Japan
(25 November 1998)

In order to gain an insight into the formation of paired Jahn-Teller (JT) stripes, we have investigated the electronic and vibronic structures in the manganese oxides by paying due attention to the effect of the Berry phase associated with the JT distortions on the band motion of an e_g electron. In terms of a band-insulator picture, we have succeeded in obtaining the JT stripes and the stabilization mechanism of the CE-type antiferromagnetism in agreement with experiment.

I. INTRODUCTION

In anticipation of a significant role in high-temperature superconductivity in the cuprates and colossal magnetoresistance (CMR) in the manganites, stripe ordering in the charge and/or spin densities has emerged as one of the central issues in condensed-matter physics. [1] Very recently, Mori, Chen, and Cheong have made an important contribution to this stripe physics by discovering an unexpected paired stripe structure in the mixed-valence charge-ordered insulating manganites, $La_{1-x}Ca_xMnO_3$ with $x \geq 0.5$. [2]

The fundamental building block of this new structure is a kind of sandwich; it consists of a pair of one-dimensional arrays of heavily distorted $Mn^{3+}O_6$ octahedra along b-axis and a string of much less (or non-) distorted $Mn^{4+}O_6$ octahedra between the $Mn^{3+}O_6$ stripes. Although unpaired $Mn^{3+}O_6$ stripes are also observed at $x = 0.5$ and in the temperature region in which charge ordering (CO) coexists with ferromagnetism (FM), [3] this basic three-row sandwich structure appears periodically with the mean spacing determined by the average charge density or x at temperature low enough for obtaining antiferromagnetism (AF) due to the spins of t_{2g} electrons. The area between the two adjacent sandwiches is made of only undistorted $Mn^{4+}O_6$ octahedra. Thus the area may be called "the plain".

Besides this charge ordering, it is highly probable that the orbital of e_g electrons in Mn^{3+} is ordered in such an alternate pattern as $d_{3x^2-r^2}$ in one $Mn^{3+}O_6$ charge stripe and $d_{3y^2-r^2}$ in the other (or $d_{x^2-z^2}$ and $d_{y^2-z^2}$ instead), just like the orbital ordering (OO) directly observed in $La_{0.5}Sr_{1.5}MnO_4$ with use of a synchrotron x-ray diffraction. [4]

The basic ingredients considered so far for describing the physics in these manganites include (i) strong Hund's rule coupling between t_{2g} and e_g electrons, (ii) hopping of an e_g electron between nearest-neighbor Mn sites via an intervening oxygen atom, (iii) strong electron correlation, and (iv) strong electron-phonon coupling leading to the Jahn-Teller (JT) effect connected with doubly-degenerate e_g orbitals. [5] The combination of the first and second ingredients provides the double-exchange (DE) mechanism, [6] which is known to be the key to bring about CMR, together with the point (iv). [7]

This fourth ingredient, especially, the cooperative JT effect is also expected to play an important role in forming the peculiar stripe CO/OO structure. Since two neighboring MnO_6 octahedra share an oxygen, distortion in one octahedron is transmitted to the other. [8] Thus the orbital ordering in each $Mn^{3+}O_6$ charge stripe along b-axis may be a direct consequence of this effect. However, because each stripe can be distorted in any direction without violating the self-consistent lattice deformation in the whole crystal, this effect alone cannot explain even the short-range, alternate pattern of orbital ordering between the $Mn^{3+}O_6$ stripes separated by the $Mn^{4+}O_6$ stripe in the basic sandwich structure, not to mention the long-range ordering among the basic structures which are well separated to one another by "the plain".

One may raise the third ingredient as essential for the stripe structure. In fact, it is natural to have a view that the long-range Coulomb interaction is quite important in the formation of a CO phase of any kind. At $x = 0.5$, for

*Int. J. Mod. Phys. B **12** 3437-3455 (1998).
†Present address: National High Magnetic Field Laboratory and Department of Physics, Florida State University, Tallahassee, FL 32306, USA.

example, the view provides an easy explanation as to the reason why each Mn^{3+} ion is surrounded with Mn^{4+} ions, forming a Wigner-lattice-type phase. However, this view contradicts the experimental fact that this CO phase becomes unstable, if the transfer energy of an e_g electron is reduced by partially substituting lanthanum ions with trivalent rare-earth ions. [9] Moreover, for the materials with $x > 0.5$, the distribution of Mn^{3+} ions becomes anisotropic rather than isotropic as can be expected in the Wigner lattice, indicating that the Coulomb correlation alone does not determine the stripe structure precisely.

Incidentally, these materials with $x > 0.5$ are observed to exhibit an intriguing oscillatory behavior in the amount of distortions at the Mn sites in "the plain". Of course, the absolute values of the distortions are small, but nonzero distortions in "the plain" suggest that there is a probability to find e_g electrons in the area. The above observation can be reconciled with the fact that these materials are basically insulators, if we adopt a picture of not a Mott but band insulator.

In the band picture, e_g electrons move under the influence of the potential determined self-consistently by the spatial variations in both amplitude and phase of the JT distortions at each Mn site. We call the phase of the JT distortion "the Berry phase" which induces an additional phase to the e_g-electron wave function. The importance of this Berry phase in the band motion has been stressed recently. [10] As a work subsequent to the previous one, we propose in this paper that a clear view can be obtained as to stripe physics in the mixed-valence manganites if we add the Berry phase as a new ingredient.

The Berry-phase connection correlates the direction of distortions at different Mn sites and this connection prevails even in "the plain", leading to a possibility to explain the long-range correlation among stripes. We can also show that the interference effect in the e_g-electron wave function provides interesting oscillations in the amount of distortions at the Mn sites. The oscillation pattern depends on the winding number w, a notion specific to the Berry phase, of the state considered. We mention that the experimentally observed situation corresponds to some particular value of w.

We start with the model Hamiltonian based on which we investigate the state exhibiting the paired JT stripes. We are mainly concerned with the material of $x = 0.5$, because most detailed information including the spin alignment of t_{2g} electrons in the AF phase is provided in this case. Comparison of total energies is made for various states specified by several indices including w in order to search the ground state of the system. We find, among others, that at $x = 0.5$ the paired JT stripe structure is obtained as the ground state and that the state is associated with the CE-type AF structure in good agreement with experiment. Then we make a detailed analysis of the state so as to show clearly how the Berry phase has an effect on the shape of the wave function. The stripe structures for both $x = 2/3$ and $3/4$ are also studied.

II. MODEL HAMILTONIAN

The fundamental elements in the physics of the manganese oxides have already been enumerated in Sec. 1. It is easy to write down the Hamiltonian taking these ingredients into account, [12,13] but such a general Hamiltonian cannot be solved practically for the study of the case with $x > 0.5$ in which the primitive cell is large. Thus some simplification is inevitable.

First-principles band-structure calculations indicate that the Hund's rule coupling has the largest characteristic energy, or the Mn d exchange splitting of about 3.5eV, among these ingredients. [11] Thus in this paper, we only consider the situation in which the spin of each e_g electron at a Mn site aligns completely in parallel with the spin direction of t_{2g} electrons at the same Mn site. In this sense, the spin degrees of freedom are lost for e_g electrons. We treat the spins of t_{2g} electrons classically. Namely, we assume several configurations of those spins first and then at each configuration we calculate the total energy of e_g electrons, keeping the t_{2g} spins intact, to find the lowest-energy configuration. The configurations considered include FM, or all spins in one direction, and several varieties of AF in which half of the spins are in one direction and the other half in an opposite direction.

Due to the absence of spin degrees of freedom for e_g electrons, we need not include the on-site intra-band Coulomb interaction. We do not consider the inter-band Coulomb interaction, either, because its main effect is to reduce a probability to occupy both e_g orbitals, but to a considerable extent it is taken care of by the JT energy stabilization. In these circumstances, we may write the effective Hamiltonian H describing the quantum mechanics of e_g electrons as [14]

$$H = -\sum_{\mathbf{j},\mathbf{a}} \mathbf{d}^\dagger_{\mathbf{j}+\mathbf{a}} T^{\mathbf{a}} \mathbf{d}_{\mathbf{j}} + \sum_{\mathbf{j}} A \mathbf{d}^\dagger_{\mathbf{j}} (Q_{2\mathbf{j}}\tau_x + Q_{3\mathbf{j}}\tau_z)\mathbf{d}_{\mathbf{j}} + \sum_{\mathbf{j}} \frac{\omega_0}{2}(Q^2_{2\mathbf{j}} + Q^2_{3\mathbf{j}}) + H_{\rm L}, \quad (1)$$

where $\mathbf{j}$ denotes the site of a MnO_6 octahedron, $\mathbf{d}_{\mathbf{j}} \equiv (d_{\mathbf{j}a}, d_{\mathbf{j}b})$, $d_{\mathbf{j}a}$ and $d_{\mathbf{j}b}$ are, respectively, annihilation operators for electrons in the states stemming from $d_{x^2-y^2}$ and $d_{3z^2-r^2}$ orbitals at site $\mathbf{j}$, $\mathbf{a}$ the vector connecting the nearest neighbor sites, and $T^{\mathbf{a}}$ the matrix describing the hopping motion in the direction of $\mathbf{a}$ with its elements as

$$t^x_{aa} = t^y_{aa} = \frac{3}{4}t, \ t^x_{bb} = t^y_{bb} = \frac{1}{4}t,$$
$$-t^x_{ab} = -t^x_{ba} = t^y_{ab} = t^y_{ba} = \frac{\sqrt{3}}{4}t. \quad (2)$$

Here t sets a unit for the hopping integral obtained by the overlap integral between adjacent $d_{3z^2-r^2}$ orbitals situated in the z-direction. [13,15]

The second term of Eq. (1) denotes the electron-lattice coupling in which A is the coupling constant, τ_x and τ_z are the Pauli matrices, and $Q_{2\mathbf{j}}$ and $Q_{3\mathbf{j}}$ are normal vibrational modes at site $\mathbf{j}$, given by

$$Q_{2\mathbf{j}} = \frac{\delta X_{\mathbf{j}} - \delta Y_{\mathbf{j}}}{\sqrt{2}}, \; Q_{3\mathbf{j}} = \frac{2\delta Z_{\mathbf{j}} - \delta X_{\mathbf{j}} - \delta Y_{\mathbf{j}}}{\sqrt{6}}, \tag{3}$$

where $\delta X_{\mathbf{j}}$, $\delta Y_{\mathbf{j}}$, and $\delta Z_{\mathbf{j}}$ represent variations in the distance between neighboring oxygens at site $\mathbf{j}$ in x, y, and z-directions.

In the third term of Eq. (1), ω_0 is the vibrational energy. Since we consider static distortions in the adiabatic approximation, the kinetic-energy term of the lattice is not included. The breathing mode, expressed as

$$Q_{1\mathbf{j}} = \frac{\delta X_{\mathbf{j}} + \delta Y_{\mathbf{j}} + \delta Z_{\mathbf{j}}}{\sqrt{3}}, \tag{4}$$

is not included, either.

The final term of Eq. (1) represents the energy loss due to the coupling of the lattice distortions with the "environment". A precise expression for the "environment" is hard to give, but we tentatively assume a phenomenological form for $H_{\rm L}$ as

$$H_{\rm L} = \frac{K_\parallel}{2}\left[\left(\sum_{\mathbf{j}} \delta X_{\mathbf{j}}\right)^2 + \left(\sum_{\mathbf{j}} \delta Y_{\mathbf{j}}\right)^2\right] + \frac{K_\perp}{2}\sum_{\mathbf{j}} \delta Z_{\mathbf{j}}^2, \tag{5}$$

where $K_\parallel$ and $K_\perp$ are, respectively, the elastic constants for dilation and compression in xy-plane and z-direction. The first term suppresses the overall deformation of MnO_6 octahedra in ab-plane, while the second quenches the distortion of a MnO_6 octahedron in c-axis. Because of asymmetry of the observed stripe structure, $H_{\rm L}$ is taken in an apparent asymmetric form between xy-plane and z-direction.

III. DRESSED OPERATOR AND THE WINDING NUMBER

In order to separate amplitude and phase of the lattice distortion, we write $Q_{2\mathbf{j}}$ and $Q_{3\mathbf{j}}$ in polar coordinates as $Q_{2\mathbf{j}} = Q_{\mathbf{j}} \sin\theta_{\mathbf{j}}$ and $Q_{3\mathbf{j}} = Q_{\mathbf{j}} \cos\theta_{\mathbf{j}}$. Using $\theta_{\mathbf{j}}$, we can introduce new operators for e_g electrons as $\tilde{\mathbf{d}}_{\mathbf{j}} = R(\theta_{\mathbf{j}})\mathbf{d}_{\mathbf{j}}$, where $R(\theta_{\mathbf{j}})$ is a unitary matrix, defined by

$$R(\theta_{\mathbf{j}}) = e^{i\theta_{\mathbf{j}}/2}\begin{pmatrix} \cos[\theta_{\mathbf{j}}/2] & \sin[\theta_{\mathbf{j}}/2] \\ -\sin[\theta_{\mathbf{j}}/2] & \cos[\theta_{\mathbf{j}}/2] \end{pmatrix}. \tag{6}$$

We note that the phase factor $e^{i\theta_{\mathbf{j}}/2}$ is needed for the assurance of single-valuedness of the electron basis for the 2π-rotation in phase of the local distortion. This is the direct effect of the Berry phase on the electron system. If we neglect this phase, the sign change of electron basis functions occurs, which makes it difficult to solve the Schrödinger equation in a consistent way.

The phase-dressed operator, $\tilde{\mathbf{d}}_{\mathbf{R}}$, naturally introduces a connection form, "the Berry-phase connection", as [16]

$$\begin{aligned} A d\mathbf{r} &\equiv \begin{pmatrix} i\langle \mathrm{vac}|\tilde{d}_{a\mathbf{R}}\nabla\tilde{d}^\dagger_{a\mathbf{R}}|\mathrm{vac}\rangle\cdot d\mathbf{r} & i\langle \mathrm{vac}|\tilde{d}_{a\mathbf{R}}\nabla\tilde{d}^\dagger_{b\mathbf{R}}|\mathrm{vac}\rangle\cdot d\mathbf{r} \\ i\langle \mathrm{vac}|\tilde{d}_{b\mathbf{R}}\nabla\tilde{d}^\dagger_{a\mathbf{R}}|\mathrm{vac}\rangle\cdot d\mathbf{r} & i\langle \mathrm{vac}|\tilde{d}_{b\mathbf{R}}\nabla\tilde{d}^\dagger_{b\mathbf{R}}|\mathrm{vac}\rangle\cdot d\mathbf{r} \end{pmatrix} \\ &= \frac{1}{2}\begin{pmatrix} \nabla\theta\cdot d\mathbf{r} & -i\nabla\theta\cdot d\mathbf{r} \\ i\nabla\theta\cdot d\mathbf{r} & \nabla\theta\cdot d\mathbf{r} \end{pmatrix}, \end{aligned} \tag{7}$$

where $|\mathrm{vac}\rangle$ denotes the vacuum state.

Due to the two-dimensional (2D) character of the stripe structure, we only consider a 2D sheet of the JT crystal in the present work. In two space dimensions, there is a topologically conserved current for an arbitrary vector field $\mathbf{v}$ as

$$j^\mu = \frac{1}{2\pi}\sum_{\nu,\lambda} \epsilon^{\mu\nu\lambda}\partial_\nu v_\lambda, \tag{8}$$

where $\epsilon^{\mu\nu\lambda}$ is the antisymmetric Levi-Civita tensor. This current obeys the continuity equation, expressed as

$$\sum_\mu \partial_\mu j^\mu = 0, \tag{9}$$

Therefore, if j^1 and j^2 are zero at the boundary of a closed surface S, the quantity Q, defined by

$$Q \equiv \int_S d^2\mathbf{r}\; j^0, \tag{10}$$

is conserved, where indices $1, 2$ indicate the space-components and 0 indicates the time-component of a vector, respectively.

For time-independent solutions with which we are concerned now, we have $\partial_0 j^0 = 0$. Thus Q is conserved for an arbitrary surface S. Substituting $\mathbf{a} = \mathrm{Tr}(A) = \nabla\theta$ for $\mathbf{v}$ into Eq. (8), we obtain the topologically conserved quantity, or "the winding number" as

$$\begin{aligned} w &= \int_S d^2\mathbf{r}\; j^0 = \frac{1}{2\pi}\int_S d^2\mathbf{r}(\partial_1 a_2 - \partial_2 a_1) \\ &= \frac{1}{2\pi}\oint_{\partial S} d\mathbf{r}\cdot\mathbf{a} = \frac{1}{2\pi}\oint_{\partial S} d\mathbf{r}\cdot\nabla\theta = m, \end{aligned} \tag{11}$$

where m is an integer representing the number for the twisting-around of the JT distortions along a path, ∂S, enclosing S. Because of the conserved nature, we will use the winding number w to label a state hereafter.

Nonzero winding number means the multiple-valuedness of θ. Therefore care must be taken for consistent assignment of θ at each site. Although θ may be multiple-valued, $\nabla\theta$ is always single-valued. Thus it is more convenient to specify $\nabla\theta$ between two neighboring sites. In a 2D square lattice in xy-plane, we can assign

$-\pi < \partial_x\theta \le \pi$ ($-\pi < \partial_y\theta \le \pi$) in x- (y-) direction for each bond. Then, giving a value of θ at a certain site automatically determines θ-values at all other sites, including their multi-valuedness.

By using $\tilde{\mathbf{d}}_{\mathbf{j}}$ thus introduced, the Hamiltonian (1) is now reduced to

$$H = -\sum_{\mathbf{j},\mathbf{a}} \tilde{\mathbf{d}}^{\dagger}_{\mathbf{j}+\mathbf{a}} \tilde{T}^{\mathbf{a}}_{\mathbf{j}+\mathbf{a},\mathbf{j}} \tilde{\mathbf{d}}_{\mathbf{j}} + E_{\rm JT} \sum_{\mathbf{j}} (2q_{\mathbf{j}}\rho_{\mathbf{j}} + q_{\mathbf{j}}^2) + H_{\rm L}, \quad (12)$$

where $\tilde{T}^{\mathbf{a}}_{\mathbf{i},\mathbf{j}} = R(\theta_{\mathbf{i}}) T^{\mathbf{a}} R(-\theta_{\mathbf{j}})$, $\rho_{\mathbf{j}} = \tilde{d}^{\dagger}_{a\mathbf{j}}\tilde{d}_{a\mathbf{j}} - \tilde{d}^{\dagger}_{b\mathbf{j}}\tilde{d}_{b\mathbf{j}}$, $E_{\rm JT} \equiv A^2/(2\omega_0)$ is the static JT energy, and $q_{\mathbf{j}} = (\omega_0/A)Q_{\mathbf{j}}$ is the dimensionless lattice deformation. The distortion part, $H_{\rm L}$, is cast into

$$H_{\rm L} = E_{\parallel}\Big[\big(\sum_{\mathbf{j}} \delta x_{\mathbf{j}}\big)^2 + \big(\sum_{\mathbf{j}} \delta y_{\mathbf{j}}\big)^2\Big] + E_{\perp} \sum_{\mathbf{j}} \delta z_{\mathbf{j}}^2, \quad (13)$$

where $E_{\parallel} = K_{\parallel}A^2/(2\omega_0^2)$ and $E_{\perp} = K_{\perp}A^2/(2\omega_0^2)$. The distance between neighboring oxygens is characterized by the dimensionless quantities, $\delta x_{\mathbf{j}} = \sqrt{2/3} q_{\mathbf{j}} \cos(\theta_{\mathbf{j}} - 2\pi/3)$, $\delta y_{\mathbf{j}} = \sqrt{2/3} q_{\mathbf{j}} \cos(\theta_{\mathbf{j}} - 4\pi/3)$, and $\delta z_{\mathbf{j}} = \sqrt{2/3} q_{\mathbf{j}} \cos\theta_{\mathbf{j}}$. Remember that $Q_{1\mathbf{j}}$ is kept to be zero.

IV. RESULTS IN THE FERROMAGNETIC CONFIGURATION

In this section, we assume the FM state in which all the spins of t_{2g} electrons align in one direction. Thus the Hund's rule coupling does not give any restriction on the hopping motion of an e_g electron. Note that the paramagnetic (PM) state may be treated in the same way as the FM state with the understanding that the hopping integral between the nearest-neighbor Mn sites, $t\cos(\varphi/2)$ with φ the relative angle between the t_{2g} spins of those Mn sites, is averaged to give a reduced value $(2/\pi)t$. We consider it reasonable to take such an average, because the e_g electrons move over a wide range compared with the lattice constant a_0 in a band picture.

A. Mean-field approximation

As shown in Fig. 1, we choose a rectangle of the size $(M/2) \times 1$ in units of $\sqrt{2}a_0$ as the unit cell in ab- (or xy-)plane relevant to the observed paired JT stripe structure. Note that M, a number of Mn sites contained in the rectangle, is related to the electron filling n as $M = 2/n$, where n is, in turn, related to x as $n = 1 - x$. For the time being, we assume the periodic boundary condition in both a- and b-directions.

In order to determine the amplitude of distortions for a given set of phases $\{\theta_{\mathbf{j}}\}$ in the unit cell, we employ the mean-field approximation to the electron-lattice coupling by the following decoupling scheme in the second term of Eq. (12).

$$q_{\mathbf{j}}\rho_{\mathbf{j}} \to \langle q_{\mathbf{j}}\rangle \rho_{\mathbf{j}} + q_{\mathbf{j}}\langle\rho_{\mathbf{j}}\rangle - \langle q_{\mathbf{j}}\rangle\langle\rho_{\mathbf{j}}\rangle. \quad (14)$$

By combining the potential term for distortions with the electron-lattice coupling term, we can easily obtain an optimized lattice distortion $q_{\mathbf{j}}^{\rm opt}$. Since $\langle\rho_{\mathbf{j}}\rangle$ is in turn dependent on $q_{\mathbf{j}}^{\rm opt}$, we have a self-consistent problem.

Because the static JT energy, $E_{\rm JT}$, is believed to be large compared with the hopping energy of an e_g electron in the manganese oxide, we take $E_{\rm JT} = 4t$ as a typical example. As for $E_{\perp}$ and $E_{\parallel}$, we choose $E_{\perp} = E_{\parallel} = E_{\rm JT}$ for simplicity. The obtained results are found to be insensitive to some particular choice of those parameters as long as $E_{\rm JT}$ is set to be larger than t.

A variety of solutions can be obtained by this self-consistent procedure in the mean-field approximation. Thus we classify the solutions using the four parameters composed of two phases θ_1 and θ_2 for heavily distorted sites in each stripe, distance between stripes d, and winding number w (see Fig. 1). The winding number is determined once $\{\theta_{\mathbf{j}}\}$ is assigned, but the assignment is a subtle matter, because it is intimately connected with the motion of e_g electrons. Apparently the motion in "the plain" is different from that in the stripe region. This suggests that a different rule should apply in each region. After several trials, we find it sensible to take the following procedure. As a first step, we make a thorough search for the distribution of $\{\theta_{\mathbf{j}}\}$ in the stripe region to obtain the optimized solution. The details in "the plain" are immaterial in the optimization procedure because of the scarceness of e_g electrons in the region. The next step is to determine the details in "the plain" on the assumption that the phase changes uniformly in the region. We deem this uniformness assumption essentially correct; it is consistent with the fact that the charge distribution of e_g electrons in "the plain" is uniform.

B. Formation of paired JT stripes

Let us consider the optimal state in the stripe region first. This amounts to the determination of the phases θ_1 and θ_2 as well as d. In Fig. 2 in which we take $n = 1/2$ with $d = 2$ and $w = 1$, the total energies are shown as a function of θ_2 for several values of θ_1. We see that the energy is optimized for the condition $\theta_1 = \pi/2$ and $\theta_2 = 3\pi/2$ (or equivalently, $\theta_1 = 3\pi/2$ and $\theta_2 = \pi/2$). We find that this optimum condition is always obtained, irrespective of n, d, or w. This universality about the condition for θ_1 and θ_2 is brought about by the following two effects. (i) Constraint in ab-plane imposed by the $H_{\rm L}$ term leads the anti-phase deformation in the heavily distorted sites, implying that $|\theta_1 - \theta_2| = \pi$. (ii) Suppression of the deformation along the z-direction gives the distortion with either $\pi/2$ or $3\pi/2$. In this way, we

have naturally obtained the orbital pattern of paired JT stripes through the optimization with respect to θ_1 and θ_2.

The fine structure of distortions inside the stripe region can be investigated by plotting the energies obtained at $\theta_1 = \pi/2$ and $\theta_2 = 3\pi/2$ (the optimized energies with respect to θ_1 and θ_2) for several sets of $\{d, w\}$. The results are shown in Figs. 3(a)-(c) corresponding to $M = 4, 6$, and 8, ($x = 1/2, 2/3$, and $3/4$) in which the energies are given as a function of the winding number w for $d = 1, 2, \cdots, M/2$. We immediately find that a state with $d = 1$ provides an energy definitely higher than that with d larger than unity. The scale for this energy separation is about $t/10$. The case of $d = 1$ is nothing but the situation in which the distorted sites come in a contiguous way, a favorable state if the cooperative JT effect dominates. It is true that the cooperative JT effect is important at half-filling, i.e., $x = 0$, in which all the sites are heavily distorted, but it does not seem to be the case when the mobile carriers exist as in the case of $x > 0$. The distortions in adjacent sites imply an electron localization in a very narrow region, which amounts to too much loss in the kinetic energy.

At $x = 1/2$, there are only two kinds of stripe structures, characterized by either $d = 1$ or $d = 2$, and the latter is stabilized in good agreement with experiment. For $x = 2/3$ and $3/4$, i.e., $M = 6$ and 8, the lowest energy is not obtained at $d = 2$ but at $d = M/2$ in disagreement with experiment. However, we may regard the states with $d > 1$ as quasi-degenerate; the difference in energies is at most $t/100$, which may be about 10^{-3}eV in manganese oxides. This energy difference is small compared to temperatures (≈ 100K) performed in the experiments. Other effects missing in our model Hamiltonian, such as a shift of the position of the manganese ion and the change of the hopping energy due to the buckling of Mn-O bond, may well lift the quasi-degeneracy in such a way as to provide the state with $d \neq M/2$ as the ground state. We point out that this is also a subtle matter from an experimental side; before performing the high-resolution experiment, a tentative conclusion was that the ground state might be the stripes with not $d = 2$ but $d = 3$ for $x = 2/3$. [17]

C. Oscillation in "the plain"

Now we pay our attention to the electronic as well as the vibronic structure in "the plain" for the state observed in the experiment, i.e., the state with $d = 2$. For $x = 1/2$, we find that the state with $w = 1$ provides the lowest energy, though the difference in energy between the states with $w = 1$ and $w = 2$ is small, i.e., at most $t/100$. For the case of $d = 2$ and $w = 1$, the orbital density together with the amplitude of distortions is shown in Fig. 4. The orbital is depicted in xy-plane and its size is drawn in proportion to the e_g-electron density $\langle \tilde{d}^\dagger_{b\mathbf{j}} \tilde{d}_{b\mathbf{j}} \rangle$. In lines with $\theta_1 = \pi/2$ and $\theta_3 = 3\pi/2$, the orbitals extending to x- and y-directions can be seen, respectively. We emphasize that asymmetry in q_2 and q_4, a peculiar feature seen in the experiment, [2,3] is reproduced.

A similar calculation is done for $M = 6$ ($x = 2/3$) with $d = 2$. Note that the pattern in the lattice distortion appears periodically in terms of w in modulo 4 in this case. As seen in Fig. 5(a), the structure in the stripe region changes only little with the change of w. However, in "the plain", we find nontrivial fine structures in the lattice distortion depending sensitively on the winding number w, as shown in Fig. 5(b). Specifically with $w = 2$, we can reproduce the same oscillatory behavior in the lattice distortion as that observed in the experiment. The corresponding orbital density is shown in Fig. 5(c). Similar results for $x = 3/4$ with $d = 2$ are given in Fig. 6(a). Here the experimentally observed oscillation pattern in $q_{\mathbf{j}}$ in "the plain" is reproduced with the state with $w = 3$. The orbital density for this case is shown in Fig. 6(b).

To conclude the results obtained so far, the oscillatory behavior in the lattice distortion corresponding to the experimental situation is a characteristic feature of the state with $d = 2$ and w, specified as

$$w = \frac{M}{2} - 1 = \frac{x}{1-x} = \frac{\text{Number of } \mathrm{Mn}^{4+} \text{ ions}}{\text{Number of } \mathrm{Mn}^{3+} \text{ ions}}, \quad (15)$$

in our model. The relation in Eq. (15) alludes some geometrical condition for the paired JT stripe structures observed in the experiment. If we solve Eq. (15) in terms of x, we obtain $x = w/(1+w)$, indicating that there exists a series of preferred values of x as $\frac{1}{2}, \frac{2}{3}, \frac{3}{4}, \cdots, \frac{7}{8}, \cdots$. Note also that although $q_{\mathbf{j}}$ oscillates in "the plain", $\langle \tilde{d}^\dagger_{b\mathbf{j}} \tilde{d}_{b\mathbf{j}} \rangle$ does not. Namely, a nearly uniform charge density is obtained for the e_g electrons in the region. The difference in the electron distribution between the two nearly-degenerate e_g states at each Mn site produces the oscillations in the lattice distortion.

D. Effect of the Berry phase on the wave function

In order to better understand the physics in the paired JT stripes, we take a closer look at the e_g-electron wave function. Here we only discuss the wave function for the case of $M = 4$ ($x = 1/2$), $d = 2$, and $w = 1$, but the same physics applies to other cases.

Generally, the single-particle state can be written as

$$|\Psi\rangle = \sum_{j=1}^{4} (\psi_{aj} \tilde{d}^\dagger_{aj} + \psi_{bj} \tilde{d}^\dagger_{bj}) |\mathrm{vac}\rangle. \quad (16)$$

In the case of $E_{\mathrm{JT}} \gg t$, we can adopt a single-band model in the sense that only the lower e_g state in a JT splitting

is occupied at each site. Then we may write an approximate form for the lowest state $|\Psi_0\rangle$ as

$$|\Psi_0\rangle \approx \sum_{j=1}^{4} \psi_{bj} \tilde{d}_{bj}^{\dagger} |\mathrm{vac}\rangle. \tag{17}$$

By performing a Fourier transform with momentum k in a-direction, we find a good approximate expression for the ground state as

$$|\Psi_0\rangle \approx \alpha_0 |-\pi/2\rangle + \beta_0 e^{i\pi/2}|0\rangle + \beta_0 |\pi/2\rangle + \alpha_0 e^{i\pi/2}|\pi\rangle, \tag{18}$$

where α_0 and β_0 are two real numbers and the state $|k\rangle$ is defined as

$$|k\rangle \equiv \frac{1}{\sqrt{M}} \sum_j e^{ik(j-1)} \tilde{d}_{bj}^{\dagger} |0\rangle. \tag{19}$$

In order to check how good this single-band model is, we plot both α_0 and β_0 as a function of E_{JT} in Fig. 7. As E_{JT}/t increases, the sum of the weights, $2(\alpha_0^2 + \beta_0^2)$, approaches unity rather quickly, implying the validity of Eq. (18) for $E_{\mathrm{JT}} \gg t$. The same analysis is carried out for the second-lowest state which is also occupied at $x = 1/2$. We obtain a similar result for this wave function as

$$|\Psi_1\rangle \approx \alpha_1 |-\pi/2\rangle + \beta_1 e^{-i\pi/2}|0\rangle + \beta_1 |\pi/2\rangle + \alpha_1 e^{-i\pi/2}|\pi\rangle, \tag{20}$$

with two real numbers, α_1 and β_1. Obtained results for these two numbers are shown in Fig. 7.

Using Eqs. (18) and (20), we readily obtain the local charge density at site j, ρ_{bj}, as

$$\begin{aligned} \rho_{b1} = \rho_{b3} &= \frac{1}{2}\left[(\alpha_0 + \beta_0)^2 + (\alpha_1 + \beta_1)^2\right], \\ \rho_{b2} = (\alpha_0 - \beta_0)^2, \;\; \rho_{b4} &= (\alpha_1 - \beta_1)^2. \end{aligned} \tag{21}$$

Inhomogeneity in the charge distribution between the sites, 2 and 4, (the former is located in the middle row of the basic three-row sandwich structure and the latter is in "the plain") is seen to originate from the interference of electron wave functions of the states with different k's. In this context, we should pay attention to the extra phase factor, $e^{\pm i\pi/2}$, appearing in Eqs. (18) and (20). Since this phase factor is traced back to the Berry-phase connection, we can conclude that asymmetry between ρ_{b2} and ρ_{b4} is a manifestation of the Berry phase. In the spirit of the adiabatic approximation, it is well understood that the ground state can be written only in terms of the lower-energy state in a JT splitting at each site, but the effect of the higher-energy state emerges through the extra phase factor.

E. Local density of states

So far, all calculations are done under the periodic boundary condition with the unit cell defined in Fig. 1. In the one-body approximation, however, it is easy to extend our calculation so as to obtain the electronic states in the whole crystal with resort to the Bloch's theorem connecting the wave function outside the unit cell. This "band calculation" is useful to obtain the local density of states (LDOS), a quantity to clarify the difference in the electronic property between the stripe region and "the plain", although it does not provide new information about the total energy in the case of a band insulator in which detailed sum in k space is not needed.

Because we are mainly interested in the variation of LDOS in a-direction, we take care of the band motion only in that direction here for simplicity. With k, momentum in the reduced zone in a-direction, the LDOS is defined as

$$D_j(\omega) = \sum_{k,\mu} (|\psi_{aj}^{k\mu}|^2 + |\psi_{bj}^{k\mu}|^2) \delta(\omega - \varepsilon_{k\mu}), \tag{22}$$

where μ is the band index and $\varepsilon_{k\mu}$ is the one-electron eigenenergy, given by the solution of $H|\Psi_{k\mu}\rangle = \varepsilon_{k\mu}|\Psi_{k\mu}\rangle$ with

$$|\Psi_{k\mu}\rangle = \sum_j (\psi_{ja}^{k\mu} \tilde{d}_{aj}^{\dagger} + \psi_{jb}^{k\mu} \tilde{d}_{bj}^{\dagger}) |\mathrm{vac}\rangle. \tag{23}$$

In Fig. 8(a), we plot the calculated band structure in the reduced zone for $M = 6$ ($x = 2/3$), $d = 2$, and $w = 2$. In this calculation, we have used a little different value for E_{JT}/t, namely, 2, instead of 4, but this change in E_{JT}/t does not cause any qualitative difference; it is made just to facilitate the band dispersion to be noticeable. The lowest and the first-excited bands are separated from other higher bands with the band gap of the order of E_{JT}. Since we consider the case of $n = 1/3$, those two bands are fully occupied.

In Fig. 8(b), $D_j(\omega)$ is drawn at each site. Since we consider band motions only in a-direction (leading to one-dimensional bands), we obtain spurious inverse-square-root divergences at the band edges. As for the site-dependence of LDOS, a significant point is that $D_1(\omega)$ and $D_3(\omega)$ in the stripe region are much larger than those in other sites, reflecting the high local electron density in the region. A more important point is that LDOS is almost independent of site in "the plain". Roughly speaking, LDOS at a site is in proportion to the inverse of the group velocity at the site. Thus the present result indicates two facts in the hopping event: (i) An e_g electron stays much longer at the stripe site, and (ii) it visits "the plain", but the visit is short and the electron move with a nearly constant high velocity, too high to deform MnO_6 substantially.

In concluding this section, we make a comment on the dichotomy which is often mentioned in relation to the

CMR physics. The content of the dichotomy is the following: There are two competing and incompatible states in the manganese oxides. One is the metallic FM state and the other is the insulating CO and/or AF state. This dichotomy, however, does not apply if we take a view of the band insulator in which a CO state can exist in the FM background.

V. RESULTS IN THE ANTIFERROMAGNETIC CONFIGURATIONS

According to the experiment, the CO/OO state appears with the AF background of the t_{2g}-electron spins in a wide doping range at temperature below about 100 K. Especially at $x = 1/2$, the very complicated stripe spin structure, the so-called CE-type AF state, has already been observed in 1950's. [18] Its origin was discussed in terms of the competition among the covalent-bond ordering, the Madelung energy, and the JT energy. [19] It is true that such a theory can narrow down candidates considerably for the ground state out of various possible spin configurations, but it cannot single the CE-type out. By model Hartree-Fock calculations, Mizokawa and Fujimori discussed the stabilization of the CE-type due to the JT distortion. [20] Here we shall show that our theory can provide the stabilization mechanism of this CE-type structure by adding the effect of the Berry phase on the e_g-electron wave function.

Our discussion so far indicates that the motion of e_g electrons in a-direction is crucial for the formation of stripes in b-direction. An AF configuration of t_{2g}-spins affects this motion through the large Hund's rule coupling. Specifically, an e_g electron hops only between adjacent sites that have parallel t_{2g} spins. Thus our first task is to extract a fundamental hopping path in a-direction.

Consider an e_g electron at site A on the line 1 in Fig. 9 and let the electron hop in the positive a-direction. Two choices exist in the hopping direction; one is to hop in x-direction and the other in y-direction. In a periodic structure along a-axis with the period M, namely, M different lines contained in the unit cell (for the case of $M = 4$, see Fig. 9), there are 2^M different paths. Each path can be represented symbolically by a series of the hopping directions, either x or y, in the unit cell.

By imposing the periodic boundary condition for the one-dimensional motion in a-direction, we can evaluate the total energy for each path by the same procedure as employed in the previous section. The result of energy for each path is given in Fig. 10(a) in which the case of $M = 4$ ($x = 1/2$) is treated. We find that the path labeled by $(xyyx)$ with $d = 2$ provides the lowest energy among those paths. If we inspect the lobes of e_g orbitals at the $Mn^{3+}O_6$ sites along the path $(xyyx)$, we notice that they are extended in the hopping direction to lower the kinetic energy.

As for the winding number, the state with $w = 1$ has the energy of $-8.4571t$ which is a little lower than that of $-8.4566t$ for $w = 2$. Thus, though the energy difference is quite small, the state specified by the path $(xyyx)$ with $d = 2$ and $w = 1$ is obtained as the lowest state for $M = 4$ ($x = 1/2$). Incidentally, the features of the single-particle wave functions are essentially the same as those found in the previous section in spite of the fact that there is a difference in dimensionality.

Now let us consider a covering of the whole ab-plane by tiling the fundamental $(xyyx)$-paths in b-direction. All t_{2g} spins align in one direction in each path due to the Hund's rule coupling. If we take the stabilization from the antiferromagnetic interaction between t_{2g} spins into account, the spin directions become opposite for each pair of adjacent paths. Thus we obtain such an overall spin and orbital structure for the ground state as depicted in Fig. 10(b). This complicated spin configuration is nothing but the CE-type AF structure in ab-plane. Note that although the structure is complicated, its derivation is easy if we follow the procedure presented here. In this sense, we claim that the stabilization mechanism for the CE-type AF structure is clarified.

VI. SUMMARY AND DISCUSSION

Based on the spinless two-band model for e_g electrons with the JT coupling to the lattice and from a viewpoint of the band insulator, we have obtained an insight into the formation of the paired JT stripes and the CE-type AF spin structure of t_{2g} electrons. The effect on the Berry phase associated with the JT center has been precisely taken into account. We pay special attention to the e_g-electron wave function not only in the stripe region but also in "the plain". The winding number, a quantity specific to the Berry phase, corresponding to the state exhibiting the paired JT stripe structure is found to have an interesting connection with x or the e_g-electron filling.

Throughout this paper, we have considered only the case of $E_{\rm JT} > t$ and the qualitative feature is the same even though we change $E_{\rm JT}$ in that region. However, if $E_{\rm JT}$ is small compared to t, the insulating solution becomes unstable and the metallic solution appears instead. The transition is expected to occur at $E_{\rm JT}$ around t. We note that the interference effect on the e_g-electron wave function due to the Berry phase becomes more apparent in the metallic solution.

We have not considered the polaron effect explicitly. As a zeroth-order approximation, the effect can be included by using a reduced value for t. A better approximation will be to use different values for t between the stripe region and "the plain", because we anticipate a larger reduction in t in the former region due to the strong distortions of the lattice.

We have discussed the stabilization of FM and AF configurations separately. If the results for the AF configurations in Fig. 10(a) are compared with those in Fig. 3, we can see that the energy related to the e_g electrons is lower in FM than that in AF by about $0.2t$ or of the order of 200K. This is a natural result, considering the fact that the e_g electrons can move more freely in the FM environment. In order to discuss the competition between FM and AF, we need to include, at least, the interactions between the t_{2g} spins in our Hamiltonian explicitly, but this is out of the range of the present work.

Nevertheless, we add one comment on the competition between FM and AF phases. Experimentally, we need only the static magnetic field of the order of 6T or the magnetic energy of about 15K to stabilize the FM phase. This energy scale, however, is smaller by at least an order of magnitude than the characteristic energy for the formation of the CO/AF state. Thus this is a difficult problem to explain. We do not know the final resolution to this problem, but we mention that this is just the same energy scale that governs the physics in "the plain" where the winding number plays an important role in specifying the features of the wave function. Since the phase of the wave function is susceptible to the magnetic flux, the magnetic field will have a strong influence on the winding number and thus on the electronic state. This may be an important future issue to investigate.

ACKNOWLEDGMENTS

TH is grateful to E. Dagotto and S. Yunoki for discussion on the orbital ordering in the manganese oxide. YT is supported by the Mitsubishi Foundation as well as the Grand-in-Aid for Scientific Research (C) under the contract No. 10640363 from the Ministry of Education, Science, Sports, and Culture (ESSC) of Japan. HK acknowledges the research grant from ISSP, University of Tokyo. Numerical calculations are done on FACOM VPP 500/40 at the Supercomputer Center, ISSP, University of Tokyo.

[1] See, for example, B. G. Levi, Physics Today **51**, 19 (1998) and the references therein.
[2] S. Mori, C. H. Chen, and S-W. Cheong, Nature **392**, 473 (1998).
[3] S. Mori, C. H. Chen, and S-W. Cheong, Phys. Rev. Lett. **81**, 3972 (1998).
[4] Y. Murakami *et al.*, Phys. Rev. Lett. **80**, 1932 (1998).
[5] As a recent review of this field, see the papers in: "Colossal Magnetoresistance, Charge Ordering, and Related Properties of Manganese oxides", ed. by C. N. R. Rao and B. Raveau, World Scientific, Singapore, 1998.
[6] C. Zener, Phys. Rev. **82**, 403 (1951); P. W. Anderson and H. Hasegawa, Phys. Rev. **100**, 675 (1955); P. G. de-Gennes, Phys. Rev. **118**, 141 (1960).
[7] A. J. Millis, P. B. Littlewood, and B. I. Shraiman, Phys. Rev. Lett. **74**, 5144 (1995).
[8] J. Kanamori, J. Appl. Phys. **31**, 14 (1960).
[9] Y. Moritomo, A. Nakamura, S. Mori, N. Yamamoto, K. Ohoyama and M. Ohashi, Phys. Rev. B **56**, 14879 (1997).
[10] H. Koizumi, T. Hotta, and Y. Takada, Phys. Rev. Lett. **80**, 4518 (1998).
[11] W. E. Pickett and D. J. Singh, Phys. Rev. **53**, 1146 (1996); I. Solovyev, N. Hamada, and K. Terakura, Phys. Rev. Lett. **76**, 4825 (1996); S. Satpathy, Z. S. Popović, and F. R. Vukajlović, J. Appl. Phys. **79**, 4555 (1996).
[12] A. J. Millis, B. I. Shraiman, and R. Mueller, Phys. Rev. Lett. **77**, 175 (1996).
[13] S. Ishihara, J. Inoue, and S. Maekawa, Phys. Rev. B **55**, 8280 (1997);
[14] In this paper, we employ such units as $\hbar = k_{\rm B} = 1$.
[15] J. C. Slater and G. F. Koster, Phys. Rev. **94**, 1498 (1954).
[16] H. Koizumi, T. Hotta, and Y. Takada, Phys. Rev. Lett. **81**, 3803 (1998); F. Wilczek and A. Zee, Phys. Rev. Lett. **52**, 2111 (1984).
[17] C. H. Chen, S.-W Cheong, and H. Y. Hwang, J. Appl. Phys. **81**, 7391 (1997).
[18] E. O. Wollan and W. C. Koehler, Phys. Rev. **100**, 545 (1955).
[19] J. B. Goodenough, Phys. Rev. **100**, 564 (1955).
[20] T. Mizokawa and A. Fujimori, Phys. Rev. B **56**, R493 (1997).

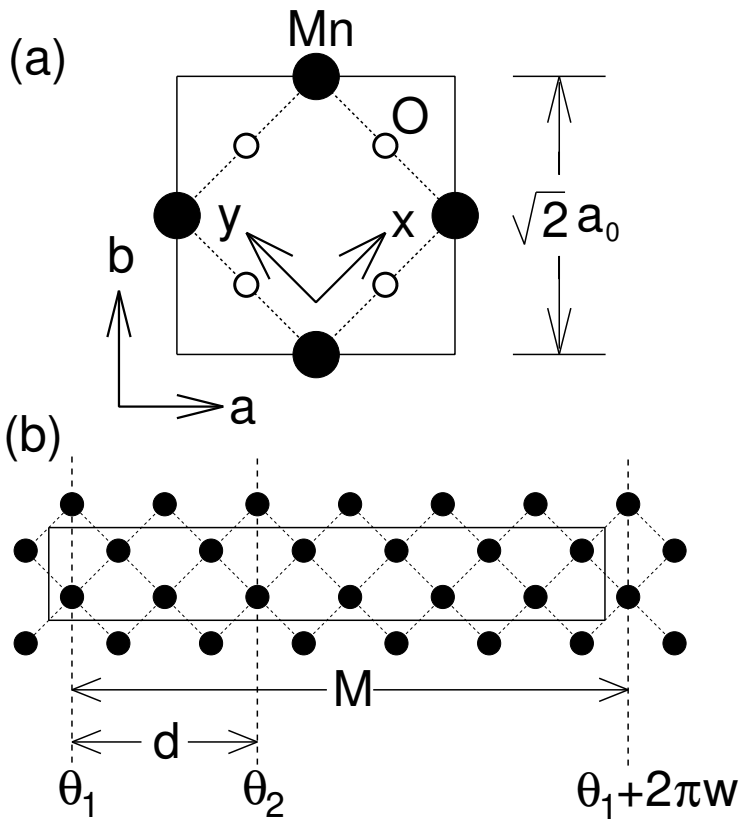

FIG. 1. 2D lattice of MnO_6 octahedra.

Our unit cell is shown by the solid-line rectangle and M represents the length along a-axis in units of $a_0/\sqrt{2}$. To specify the paired-stripe phase, we introduce four parameters: θ_1 and θ_2 are the phases at the heavily distorted sites, d is the distance between those sites in the a-direction in units of $a_0/\sqrt{2}$, and w is the winding number of the phase for the path along a-axis from a site in the cell to the equivalent site in the adjacent cell.

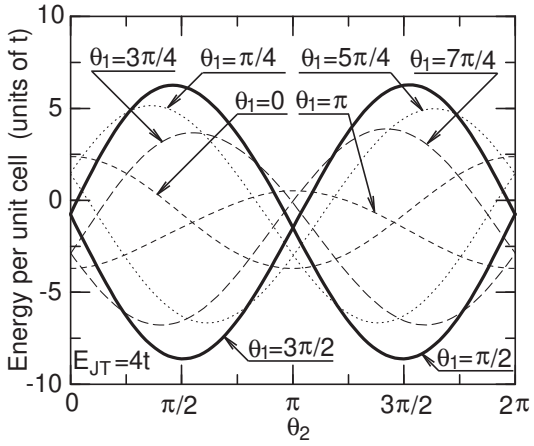

FIG. 2. Energy per unit cell as a function of θ_2 for several values of θ_1 with $M = 4$ ($x = 1/2$), $d = 2$, and $w = 1$.

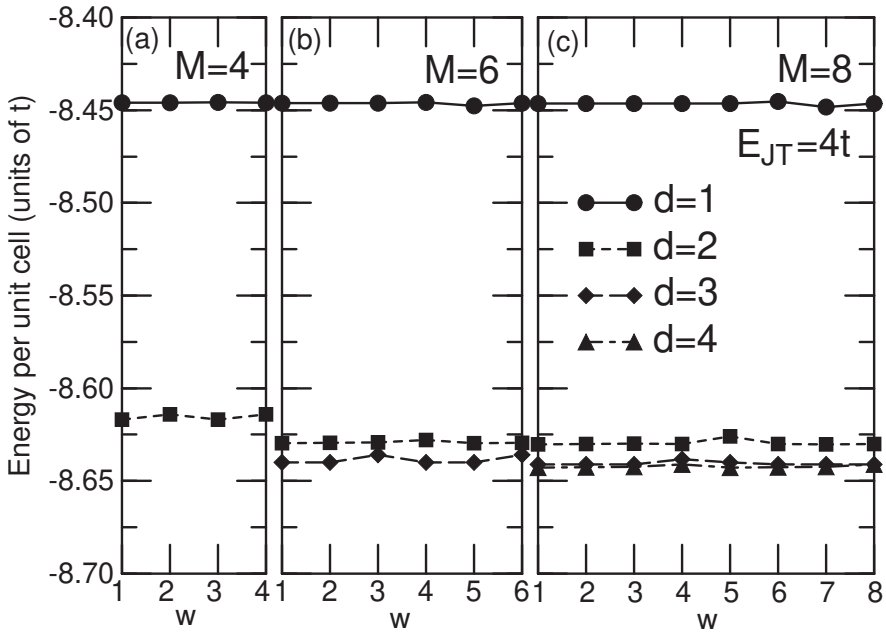

FIG. 3. Energy per unit cell as a function of the winding number w for several values of d for (a) $M = 4$ ($x = 1/2$), (b) $M = 6$ ($x = 2/3$), and (c)$M = 8$ ($x = 3/4$).

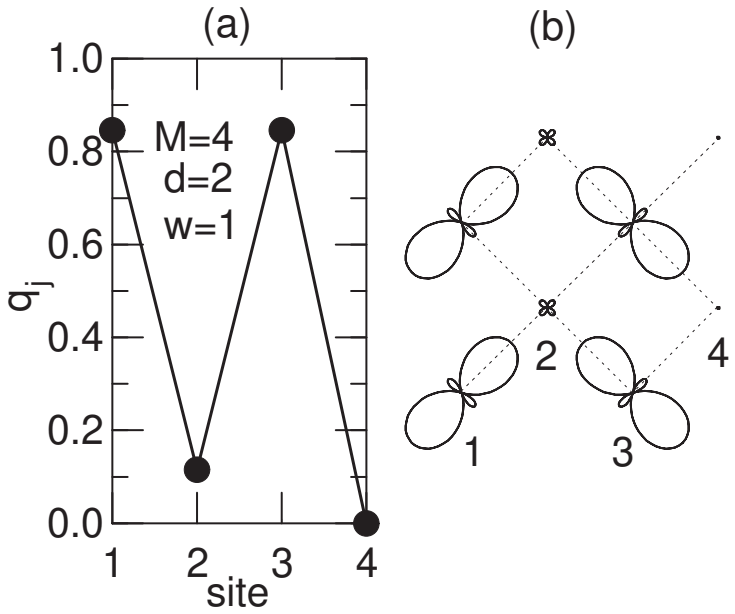

FIG. 4. (a)Dimensionless lattice distortion at various sites in the unit cell for $M = 4$ ($x = 1/2$), $d = 2$, and $w = 1$. (b)The orbital density in xy-plane. The size of the orbital is in proportion to the e_g-electron density $\langle \tilde{d}^{\dagger}_{b\mathrm{j}} \tilde{d}_{b\mathrm{j}} \rangle$.

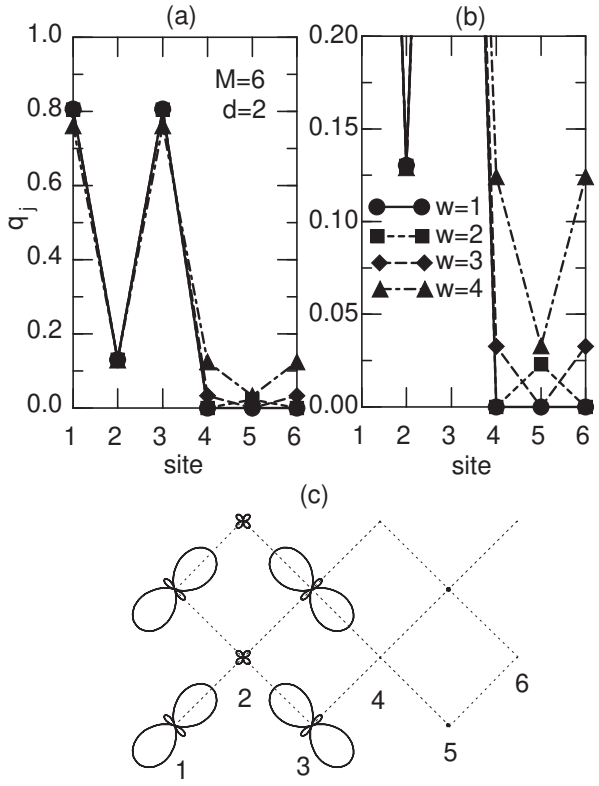

FIG. 5. (a) Dimensionless lattice distortion at various sites in the unit cell for several values of w with $M = 6$ ($x = 2/3$) and $d = 2$. (b) Same as in (a) with the vertical axis magnified. (c) The orbital-density pattern for $w = 2$.

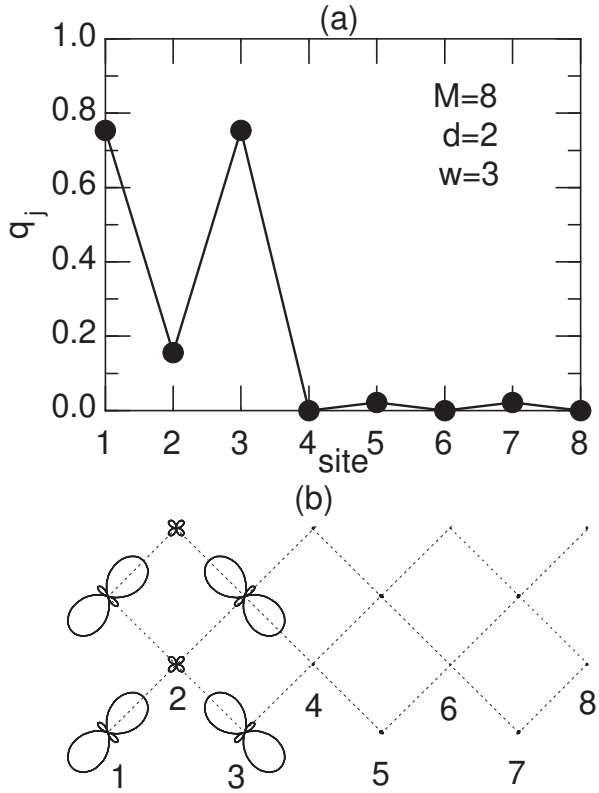

FIG. 6. (a)Dimensionless lattice distortion at various sites in the unit cell for $M = 8$ ($x = 3/4$), $d = 2$, and $w = 3$. (b) The orbital-density pattern for the same parameters as those in (a).

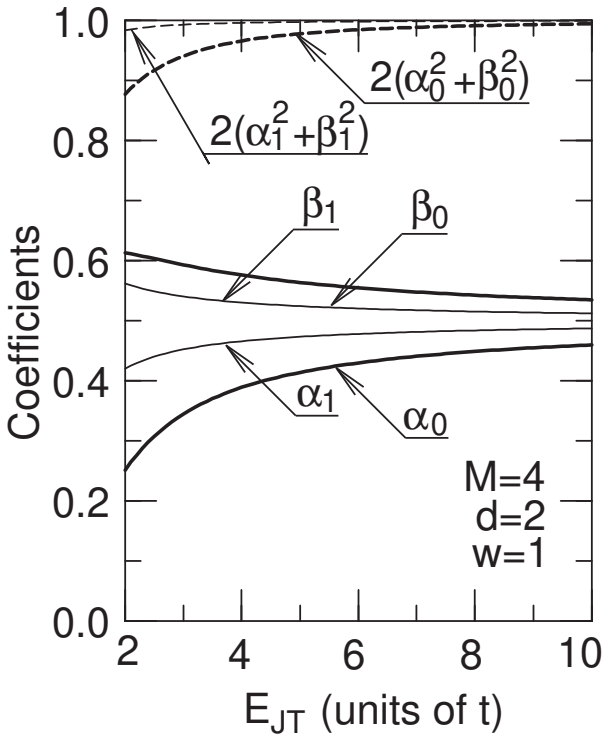

FIG. 7. Coefficients in the lowest and second-lowest single-particle wave functions plotted as a function of $E_{\rm JT}$. The broken curves denote the sums of weights.

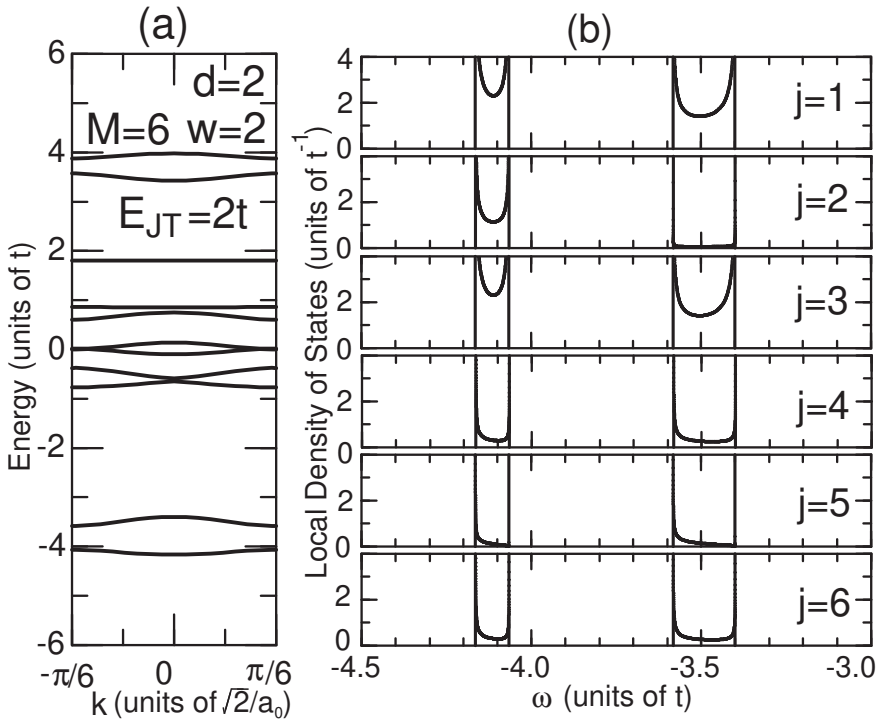

FIG. 8. (a) One-dimensional band structure. (b) Local density of states.

The case of $M = 6$ ($x = 2/3$), $d = 2$, and $w = 2$ is treated. Note that k is in units of $\sqrt{2}/a_0$.

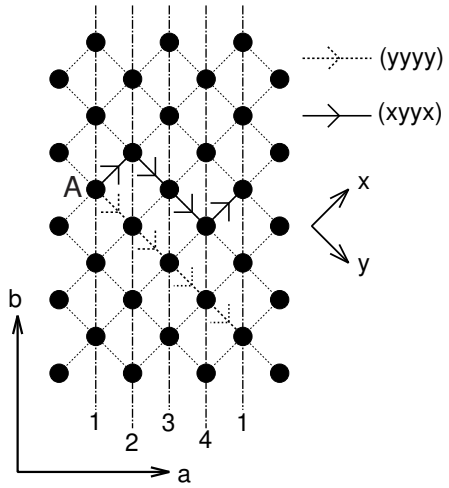

FIG. 9. Path for the hopping motion of an e_g electron from site A along a-axis. The paths indicated by solid and dashed lines are, respectively, represented symbolically as $(xyyx)$ and $(yyyy)$.

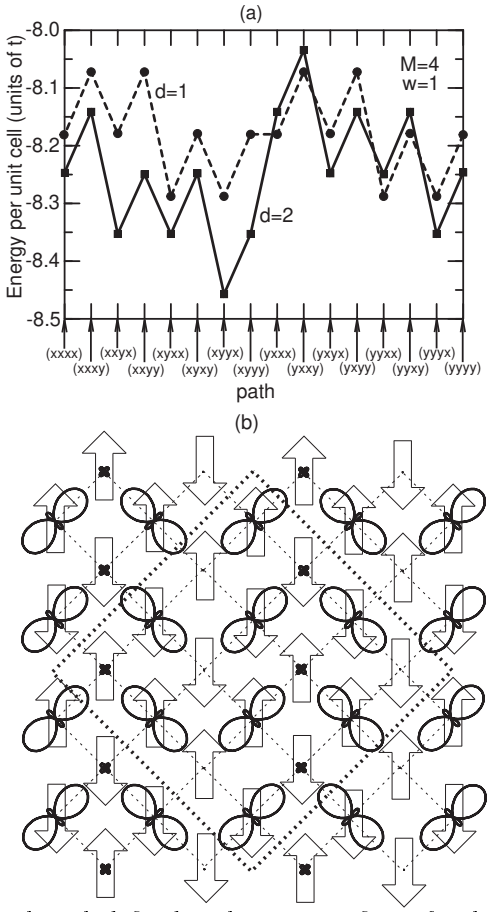

FIG. 10. (a) Energy per unit cell for each path defined in the previous figure for the case of $M = 4$ ($x = 1/2$). (b) Spin and orbital structure for the state constructed by the tiling of the fundamental $(xyyx)$-paths with the alternate up- and down-t_{2g} spins from one path to another in b-direction. The spin configuration thus obtained is found to be just the CE-type AF structure.